Analytical Methods

ARTICLE

Label-free characterization of biochemical changes within human cells under parasite attack by synchrotron based micro-FTIR

Received 00th January 20xx,
Accepted 00th January 20xx

DOI: 10.1039/x0xx00000x

www.rsc.org/

Hany M. Elsheikha*[a], Nashwa A. Elsaied[a], K.L. Andrew Chan[b], Chris Brignell[c], Mohamed S.R Harun[a, d], Katia Wehbe[e], and G. Cinquee [e]

The protozoan *Toxoplasma gondii* is responsible for severe, potentially life-threatening, infection in immunocompromised individuals and when acquired during pregnancy. In the meantime, there is no available vaccine and the anti-*T. gondii* drug arsenal is limited. An important challenge to improve antiparasitic therapy is to understand chemical changes that occur during infection. Here, we used Fourier transform infrared spectroscopy (FTIR) to investigate the effect of *T. gondii* infection on the chemical composition of human brain microvascular endothelial cells (hBMECs) at 3, 6, 24 and 48 hours postinfection (hpi). Principal component analysis (PCA) showed that the best separation and largest difference between infected and uninfected hBMECs was detected at 24 hpi and within the 3400-2800 cm^{-1} region. At 48 hpi, although the difference between samples was obvious within the 3400-2800 cm^{-1} region, more differences were detected in the fingerprint region. These findings indicate that infected and control cells can be easily distinguished. Although differences between the spectra varied, the separation was most clear at 24 hpi. *T. gondii* increased signals for lipids (2853 cm^{-1}) and nucleic acids (976 cm^{-1}, 1097 cm^{-1} and 1245 cm^{-1}), and decreased signals for proteins (3289 cm^{-1}, 2963 cm^{-1}, 2875 cm^{-1}) in infected cells compared to controls. These results, supported by amino acid levels in culture media, and global metabolomic and gene expression analyses of hBMECs, suggest that *T. gondii* parasite exploits a wide range of host-derived chemical compounds and signaling pathways for its own survival and proliferation within host cells. Our data demonstrate that FTIR combined with chemometric analysis is a valuable approach to elucidate the temporal, infection-specific, chemical alterations in host cells at a single cell resolution.

1. Introduction

The apicomplexan protozoan parasite *Toxoplasma gondii*, one of the world's most prevalent parasites, is the causative agent of toxoplasmosis, a potentially serious disease in immunocompromised individuals and when acquired during pregnancy.[1] The neuro-pathogenic parasite *T. gondii* chronically infects one-third of the world's human population.[2] At the same time, global healthcare challenges from this serious parasite are increasing due to drug resistance, low tolerance to current drug treatments and lack of vaccines.[3] *T. gondii* is an obligate intracellular parasite which causes disease by invading and replicating within human cells. Infection involves entry into the host cell followed by transition to proliferative tachyzoites, eventually differentiating into a dormant tissue cyst containing bradyzoites, which marks the chronic form of toxoplasmosis. This interaction between *T. gondii* and the host cell involves spectacular bioengineering wherein essential intracellular components, especially lipids, are hijacked from the host cell to support the parasite, despite its independent capacity to synthesize membrane lipids.[4] Intracellularly, the parasite creates and resides inside a parasitophorous vacuole (PV), a specialised compartment inside which the parasite is protected against cellular defences.

T. gondii acquires lots of nutrients from the host cellular microenvironment during infection to generate

[a] Faculty of Medicine and Health Sciences, School of Veterinary Medicine and Science, University of Nottingham, Sutton Bonington Campus, Loughborough, LE12 5RD, UK
[b] King's College London, Institute of Pharmaceutical Science, Franklin-Wilkins Building, 150 Stamford Street, London, SE1 9NH, UK
[c] School of Mathematical Sciences, University of Nottingham, Nottingham, NG7 2RD, United Kingdom
[d] Infectomics Cluster, Advanced Medical & Dental Institute, Universiti Sains Malaysia, Bertam, 13200 Kepala Batas, Pulau Pinang, Malaysia
e Diamond Light Source, Didcot, Oxfordshire, OX11 0DE, UK

Electronic Supplementary Information (ESI) available: [details of any supplementary information available should be included here]. See DOI: 10.1039/x0xx00000x

energy and biomass for survival and replication. Although nutrient uptake and utilization are the basis of the parasite's physiology, many questions related to these important biological processes, are still poorly understood. For example, what is the chemical composition of the parasite-infected host cells and how does this evolve over time? It is evident that such cellular processes involve highly orchestrated, complex time-dependent molecular interactions. Extracting quantitative information without disturbing the cell, while preserving molecular specificity remains a challenge when imaging individual cells. Conventional methods used to study *T. gondii* interaction with host cell, such as immunocytochemistry, electron microscopy, fluorescence imaging and gene expression, [5] are invasive because they require fixation, permeabilization, tagging, labelling, or even lysis. Transgenic strategies to express markers such as GFP have been developed, but require laborious protocols that can interfere with the normal behaviour of both parasites and host cells. In addition, the limited availability of genetically encoded fluorescent probes with distinct emission spectra impedes simultaneous visualization of multiple molecular species in single cells.

To improve understanding of the multifaceted nature of host cell-parasite interaction, a biocompatible, label-free approach is required to address the chemical changes that mediate host-parasite interaction. Microspectroscopy techniques such as micro-Fourier Transform IR interferometry can provide label-free chemically specific microscopy contrast based on vibrational absorption spectroscopy to reveal the distribution of distinctive molecular composition throughout an intact biological sample. [6] A recent study showed that attenuated total reflectance Fourier transform infrared spectroscopy (ATR-FT-IR) combined with multivariate analysis can distinguish early stage malarial parasite-infected cells from control cells. [7] Over the past decade, the application of this method coupled with synchrotron source has been shown to offer clear advantages for a range of biomedical research applications including chemical profiling of viral-infected cells. [8, 9] The intrinsic molecular image contrast provides label-free quantitative functional analysis, without suffering from photobleaching or radiation damaging.

The aim of this work was to exploit the unique parasite's biology and the sensitivity of Synchrotron Radiation-based IR microspectroscopy to directly characterize chemical changes that occur in blood-brain barrier endothelial cells subsequent to infection, thus obtaining new data on the pathogenesis of *T. gondii* infection. The presented approach opens new possibilities to investigate system-wide host-pathogen metabolic interaction, which can enhance understanding of the intracellular lifestyle of *T. gondii* and related pathogens.

2. Methods

2.1. Parasite strain and growth conditions

Tachyzoites of *Toxoplasma gondii* RH strain were maintained in Vero cell culture grown in 75-cm² plastic culture flasks. The inoculated cell culture was maintained in 15 ml of complete DMEM (Dulbecco's Modified Eagle Medium) at 37°C, 5% CO_2. The parasites were harvested when lysis of the Vero cells, due to infection, was completed, or until very few host cells remained intact, and a new Vero cell culture flask was inoculated in order to establish an on-going parasite culture. To harvest the parasites once nearly all of the Vero cells had been lysed by the parasite, the culture flask was gently agitated and the entire content was transferred to a 50ml falcon tube. The contents were left to settle for 10 min and any floating cell debris were removed by pipetting, being careful not to disturb the parasites towards the bottom of the solution. The tube containing the parasite was then centrifuged at 2,000*xg* for 5 min. The supernatant was carefully removed and the parasite pellet was re-suspended in 2.5ml of sterile 1 x Phosphate Buffered Saline (PBS). The parasite suspension was then purified using a PD-10 desalting column filled with Sephadex-25 gel filtration material (GE Healthcare, UK), as previously described. [10] The purified parasite material was then centrifuged at 3,000*xg* for 5 min. The supernatant was carefully removed and the purified parasite pellet was re-suspended in 5ml of culture media. An aliquot was taken to quantitate the number of parasites per millilitre using a hemocytometer.

2.2. Culture of hBMECs

Human brain microvascular endothelial cells (hBMECs) were used at passage 10 and were grown in complete RPMI-1640 Medium (cRPMI) supplemented with 20% heat inactivated fetal bovine serum (FBS), 2mM L-glutamine, 1mM

sodium pyruvate, 1% MEM nonessential amino acids, 1% MEM vitamins and 2% penicillin/streptomycin as previously described. [11] Cells were maintained in an incubator in a humidified 5% CO_2-95% air at 37°C. Once confluent (~3-5 days), cells were trypsinized using trypsin-ethylenediaminetetraacetic acid (EDTA) (Sigma-Aldrich, St. Louis, MO). Cells were considered confluent when their expansion had reached a point where cells touched each other on all sides and no intercellular gaps were observed. To rule out if cell viability could be regarded as a factor affecting parasite interaction with host cells and hence, any subsequent measurements, the viability of hBMECs was assessed on a minimum of 100 cells using trypan blue exclusion assay prior to inoculation onto culture chambers or flasks. Only cells with >98% viability were used.

2.3. Experimental infection

All work was carried out inside a BSC level II hood, under strict aseptic conditions. At approximately 90% confluence, hBMECs were harvested using trypsin-EDTA and seeded directly onto the surface of CaF2 windows (1 mm thick) by pipetting 5,000 cells dropwise. Cells were incubated under the same conditions described above for an additional 24 h prior to start of experimentation. This seeding density produced a sparse to midrange confluency (30–50%) well suited for imaging individual cells. Freshly harvested, purified *T. gondii* tachyzoites were added to hBMECs at a host-parasite ratio of 1:3 (i.e., MOI; multiplicity of infection of 3). Parallel culture chambers were mock-inoculated with medium only and used as controls. Infection was allowed to progress for up to 48 hr post infection (hpi). At 0 hr (baseline chemical profile of cells before infection), and at 3, 6, 24, and 48 hpi, three biological replicates from both infected and non-infected (controls) cells were fixed for 30 minutes in 4% buffered paraformaldehyde solution and prepared according to sample preparation protocols optimized for SR microFTIR imaging in transmission. [12] In the present study, analyzing live cells was not possible because of the perceived health risks associated with the use of live zoonotic parasites in biosafety level-1 (BSL-1) imaging facility.

2.4. MicroFTIR imaging

MicroFTIR absorbance spectra were acquired in transmission from spot areas delimited by IR microscope slits fitting the dimensions of a cell diameter ~15 μm at the Diamond Light Source synchrotron facility (MIRIAM, beamline B22). A 36x magnification objective/condenser optics were used with SR and high sensitivity MCT detector in an infrared microscope (Bruker Optics Hyperion 3000). The spectra for several individual cells were acquired in the mid-IR sampling interval from ~600 to 4000 cm^{-1} (scanner velocity of 80 kHz, spectral resolution 4 cm^{-1}) by typically co-adding 256 scans (circa 30 sec), depending on the overall cell absorbance and the necessary spectral quality).

2.5. Principal component analysis (PCA) of FTIR data

Spectral pre-processing was carried out using the OPUS software version 7.5 (Bruker Optics). FTIR spectra were first truncated into two separate spectral regions, 3400–2800 cm^{-1} and 1740–900 cm^{-1}. "atmospheric compensation" from the OPUS software was applied to remove the residue contribution from water vapor. Second derivative was then applied with 21 points smoothing followed by max-min normalization. PCA was applied to the processed spectra using the PyChem software (Version 3.0.5g Beta) package. [13] The first 12 principal components (PC) were studied in detail, but only PCs showing a clear separation between sample groups were included in the result.

2.6. Cell viability

The nonradioactive colorimetric 3-(4,5-dimethyl-2-thiazolyl)-2,5- diphenyl tetrazolium bromide (MTT, Sigma) reduction assay was employed to determine the effect of *T. gondii* infection at a MOI of 3 on the viability of hBMECs at 3, 6, 12, 24 and 48 hpi. hBMECs (10^5 cells/well) were cultured in 96-well tissue culture plates (Nunc) in 100 μl of culture medium for 18 hr in a humidified incubator (37°C, 5% CO_2) until become confluent. Tachyzoites of *T. gondii* were added, in triplicate, to hBMECs at a MOI of 3 for 2 hr, followed by removal of the medium and washing twice with fresh culture medium to remove extracellular non-attached parasites. Each well was filled with 100 μl of culture medium and the plates were further incubated. Dimethyl sulfoxide (DMSO, 0.1%) was used as control. At 3, 6, 12, 24 and 48 hpi MTT

was added to each well (to a final concentration of 0.5 mg/ml), and incubation was continued for further ~3 h in the dark at 37°C. The cells were then incubated for 1 hr in 100 µl of solubilizing solution (50% sodium dodecyl sulfate in 0.1 mM HCl). The optical density (OD) was read by a microtiter plate reader at 570nm with a reference wavelength of 690 nm. The results were expressed as a viability percentage of cell numbers compared with that of healthy control (i.e., mock-infected, control, cells at 0 hpi). The experiment was performed in triplicate. Results were analyzed with a Student's *t* test and graphs were produced using Prism (GraphPad Software, Inc.). Data are expressed as mean ± SD and a p value <0.05 was considered statistically significant.

2.7. Flow cytometry

To explore the extent of *T. gondii* influence on the host cell cycle, we performed cell cycle analysis at 3, 6, 12, and 24 hpi by measuring DNA content using propidium iodide staining as described previously.[14] Asynchronously growing *T. gondii*-infected and uninfected hBMECs were trypsinized using trypsin-EDTA. Following centrifugation (400×*g* for 10 min), the cells were fixed and permeabilized with ice-cold 70% ethanol for 60 min. Following washing with PBS, the cells were incubated with PI (100 µg/ml; Sigma) at a concentration of 10^6 cells/ml at ambient temperature in the dark for 15 min. Fluorescence emission of PI was analyzed with a Beckman Coulter Altra flow cytometer (Beckman Coulter) at 617 nm after excitation with a blue laser at 488 nm.

2.8. Targeted GC-MS profiling of extracellular amino acids

Dynamic amino acid concentration data were generated from a time-course *in vitro* experiment. Supernatant from *T. gondii*-infected and uninfected control cell cultures were collected at 0, 3, 6, 24, 48, 72, and 96 hpi and kept frozen at –80°C until analysis. Extracellular amino acids were quantified using Gas Chromatography Coupled with Mass Spectrometry (GC-MS) using an EZ-faast™ amino acid GC kit (Phenomenex Inc., Macclesfield, UK), as previously described. [15, 16] Frozen culture media were thawed on ice prior to analysis. Amino acids were isolated from samples and derivatized using the EZ:FaastTM amino acid kit according to the manufacturer's instructions (Phenomenex, Macclesfield, UK). Briefly, 25 µl of each sample were combined with 20 nmol (100 µl) norvaline, as an internal standard. This solution was passed through the EZ:Faast solid phase extraction absorbent, which was washed with 200 µl propanol. A solution of propanol and sodium hydroxide (200 µl) was then used to remove the absorbent (and the amino acids retained on it) from the pipette tip. Chloroform (50 µl) and iso-octane (100 µl) were then sequentially added to the solution to derivatize the amino acids. The amino acids were recovered in the upper organic layer, dried under a stream of nitrogen. Then, the sample was re-dissolved in 100 µl iso-octane:chloroform (80:20 v/v). For GC-MS analysis of amino acids, 1 µl of the sample was injected in splitless mode (split closed for 10 s) using an AS800 autosampler (PerkinElmer, Beaconsfield, UK). The injector of the GC8000 gas chromatograph (Fisons, Manchester, UK) was maintained at 250°C, with an initial oven temperature of 90°C, which was increased to 320°C at 20°C/min (transferline from the oven to mass spectrometer, 300°C). Helium (12 psi (82.8 kPa) was used as the carrier gas to elute the amino acids from the ZB-AAA column (10 m × 0.25 mm internal diameter). The MD800 mass spectrometer (Fisons) was operated in selected ion mode recording ions 101, 114, 116, 130, 144, 146, 155, 156, 158, 172, 180, 184, 243 and 244 with a dwell time of 0.03 s. Calibration was achieved by comparison of peak areas for the amino acids in standard and sample runs after adjustment for variation in the peak area of the internal standard. Amino acid levels in the culture medium were measured by ion-exchange chromatography. After thorough examination of the measured concentration data in terms of data quality assurance and reliability, we selected a set of 23 amino acids and considered them for data analysis. These include: alanine (ALA), sarcosine (SAR), glycine (GLY), alpha amino-butyric Acid (ABA), valine (VAL), leucine (LEU), isoleucine (ILE), threonine (THR), serine (SER), proline (PRO), asparagine (ASN), aspartic Acid (ASP), methionine (MET), hydroxyproline (HYP), glutamic Acid (GLU), phenylalanine (PHE), alpha-aminoadipic acid (AAA), glutamine (GLN), ornithine (ORN),

lysine (LYS), histidine (HIS), tyrosine (TYR), and tryptophan (TRP).

2.9. GC-MS metabolomic analysis

T. gondii-infected and uninfected host cells were collected at several time points (6hr, 24hr and 48hr) after infection. About 1 ml of cold solvent (maintained at −50°C) comprised of methanol:water in a ratio of 80:20 (v/v) was added into each flask to quench the metabolic activity of the cells. This was followed by scraping cells off the flask and centrifugation at 3,000×*g* for 10 min at 4°C. Following the centrifugation, the supernatant was removed and the cell pellets were processed for metabolite extraction. ~750 µl of cold solvent (−20 °C) were added to the cell pellet, followed by three freeze–thaw cycles to extract the intracellular polar metabolites into the polar phase. The samples were then pelleted by centrifugation (13,500×*g,* 5 min, 9 °C) and the supernatant was stored on dry ice. This procedure was performed two times on the cell pellets and both extracts were combined and kept on dry ice. Aliquots (1,400 µl) of intracellular extracts were normalized according to OD_{660}, followed by the preparation of a quality control (QC) sample.[17] Samples were derivatized for GC–MS following a two stage process. [18] The derivatized samples were analyzed using an Agilent 6890 GC and a LECO Pegasus III TOF mass spectrometer (Leco, St. Joseph, MI, USA). [17] Data analysis was performed using Metaboanalyst 3.0.

2.10. RNA isolation and microarray expression analysis

The monolayers of hBMECs were infected with purified *T. gondii* tachyzoites at a MOI of 3 for 60 min and washed, and incubation in cRPMI medium was continued for 6, 24 and 48 h before harvesting. Total RNA was extracted from *T. gondii*-infected hBMECs and control uninfected cells using RNeasyMini Kit (Qiagen). Isolated RNAs were eluted with nuclease-free water and stored at −80°C, until microarray analysis. Sample labelling and microarray (GeneChip™ Human Gene 2.1 ST, Affymetrix) analysis was performed with the support of the Arabidopsis Stock Centre (NASC), University of Nottingham. The concentration and quality of RNA were determined using the Agilent 2100 Bioanalyzer (Agilent Technologies Inc., Palo Alto, CA) and the RNA 600 Nano Kit (Caliper Life Sciences, Mountain View, CA), respectively. Samples with at least RNA concentration of 100 ng/µl and RNA Integrity Number ≥ 8 were used for gene expression analysis. Single stranded complimentary DNA was prepared from 200 ng of total RNA as per the instructions of the GeneChip™ WT PLUS Reagent Kit (Applied Biosystems and Affymetrix). RNA was converted to cDNA, followed by transcription to cRNA. Single stranded cDNA was synthesized, end labeled and hybridized for 16 h at 45°C to GeneChip™ Human Gene 2.1 ST arrays. All steps were carried out by a Gene Atlas™ Personal Microarray system (Affymetrix). Gene expression data and pathway analysis of the differentially regulated genes were analyzed using Partek Genomics Suite 7.0 software (Partek Incorporated). The raw CEL files were normalized using the RMA background correction with quantile normalization, log base 2 transformation and mean probe-set summarization with adjustment for GC content. Differentially expressed genes were considered significant if *p*-value with false discovery rate (FDR) was ≤ 0.05 and fold change of >1 or <-1. The microarray experiments were independently performed on three biological replicates.

2.11. Statistical analysis

Statistical analysis was performed using Prism, version 6.0 (GraphPad), and R, version 3.2.4. Statistical significance for cell viability and cell cycle data was determined using one-way ANOVA with Dunnett's post-test for infected cultures with the uninfected condition being the comparator for all other data. Differences in cell numbers at different cell cycle stages between infected and control cells were assessed by a Wilcoxon rank sum (Mann–Whitney U) test. To examine the effect of *T. gondii* infection on amino acid levels, multiple two-way ANOVA models were fitted, one for each amino acid, with time, treated as a factor with seven levels, and infected/control condition as the covariates and amino acid level as the response variable. We tested the null hypothesis that there was no difference in amino acid levels between control and infected cells at each time point using *t*-tests. After correcting for multiple comparisons, a

threshold of p <0.0003 was significant at the 5% significance level. For each amino acid we considered the most significant time point (the time point with the smallest p-value). A volcano plot showing the significance ($-\log_{10}$ [p value]) *versus* the effect size (the difference in amino acid levels between control and infected cells) was plotted.

A profile of each amino acid from both the control and infected cultures over the time course of the experiment was calculated by taking the mean over control replicates and infected replicates. The averages, plus and minus one standard deviation, were plotted. The average time courses were grouped according to hierarchical agglomerative clustering using Ward's method on Euclidean distances between vectors consisting of average amino acid levels over the seven time points. A heatmap of the average time courses, with the amino acids ordered according to the cluster analysis was plotted with dendrograms to show the relationships between the clusters. The dendrogram was next cut to create seven groups. The mean and standard deviation were calculated across the individual replicates, which constituted the amino acids in each group. The means for each group, plus and minus one standard deviation were plotted.

3. Results

3.1. FTIR profiling

The PCA score plots and selected loading plots (all other loading plots can be found in Fig. S1) of the spectral data in the 3400–2800 cm^{-1} region are shown (Fig. 1). This is the ν (CH), ν (NH) and ν (OH) region. The ν (OH) band has a broad feature which is diminished by the 2nd derivative procedure, therefore the focus in this region is at the ν (CH) and ν (NH) vibrational mode. A clear differentiation between the infected group (red squares) and control group (blue dots) are detected at all time points after infection. At 3 hpi, the score plot (Fig. 1a) shows that the main separation was found along the y-axis (PC6). However, this PC only accounts for 1.21% of the variance suggesting the difference between the two groups is small. At 6 hpi, the score plot (Fig. 1b) shows that separation can be found along the y-axis (PC2) with 16.9% of the variance and the control mostly had a positive score while the infected had a negative score. The corresponding PCA loading on the y-axis of the score plot (Fig. 1c) shows the protein ν (NH) peak at 3289 cm^{-1}, ν (CH_3) at 2963 cm^{-1} and 2875 cm^{-1} are in the positive region whereas the lipid ν (CH_2) peak at 2853 cm^{-1} was negative. Since these loadings are based on 2nd derivative spectra, the PCA shows that cell protein concentration relative to lipid has decreased when the cells are infected. A similar pattern was also observed in the 48 hpi data (Fig.1e and f) with 10.32% variance. Interestingly, when data from all time points after infection were analyzed all-together, the score plot (Fig. 1g) showed a clear difference between the control and the infected groups from PC5, and the data from 6 hpi (blue triangles) and 48 hpi (x) from (PC2) with the corresponding PC loading (Fig. 1h) shared the same pattern as Fig. 1c and f. These results indicate that changes in the protein and lipid ratio are mostly observed between 6 and 48 hpi.

The results of the PCA of the region from 1740 cm^{-1} to 900 cm^{-1} are shown in Fig. 2. This region contains major IR bands associated with protein amide I (~1654cm^{-1}), II (1544 cm^{-1}) and III (1240 cm^{-1}), ν (COO^-) (~1600 cm^{-1} and ~1400 cm^{-1}), δν CH (1454 cm^{-1}), ν (PO_2^-) (~1225 cm^{-1} and ~1090 cm^{-1}) and other carbohydrates ν (C-O) vibrations between 1300-1000 cm^{-1}. The 2nd derivative spectrum is therefore complex, which results in the complex patterns observed in the PC loadings shown (Fig. S2). Nevertheless, clear separation between the infected group (red squares) and control group (blue dots) can be observed and the separation became clearer as the time after infection progresses. This was not observed when analyzing the 3400-2800 cm^{-1} region. Importantly, when data from all time points after infection are analyzed together, the score plot (Fig. 2e) along the x-axis (corresponding PC shown in Fig. 2f) shows a progressive transition from the negative side to the positive side as a function of time after infection. The PC loading in Fig. 2f shows that there is residue water vapor in the background, which the software did not subtract completely. The water vapor prevented direct observation of the changes in the protein amide I and II bands. However, there were clear changes in the amide III region where a derivative shape was observed, which is indicative of a shift of the amide III band. Further restriction of the spectral region to 1400–900 cm^{-1} in the PCA produced a similar result suggesting that the remaining water vapor peak did not interfere with the analysis. Amide III is known to be

sensitive to the secondary structure of protein where a shift towards 1250–1220 cm^{-1}, as in this case with an increase in time after infection, is indication of increase in beta-sheets structure. [19, 20] Apart from the potential slight change in the secondary structure of protein, the loading of the combined PCA that separated the control, with a negative score, from all the infected groups (Fig. 2g) had shown three distinct negative peaks at 976 cm^{-1}, 1097 cm^{-1} and 1245 cm^{-1}. These three peaks are very close to the characteristic nucleic acid bands, normally found at 970 cm^{-1}, 1087 cm^{-1} and 1240 cm^{-1}, suggesting that the infected cells had a relatively higher nucleic acid content than the control cells.

The PCAs of the spectra of the uninfected cells in the infected culture against cells in the uninfected control culture are shown in Fig. 3. Clear separation can be observed in both the 3400-2800 cm^{-1} region (Fig. 3a) and the 1740-900 cm^{-1} region (Fig. 3c). However, the variance in the 3400-2800 cm^{-1} region was relatively small at 1.42%, whereas the variance in the 1740-900 cm^{-1} was much higher at 64.9%, suggesting most of the changes are found in the 1740-900 cm^{-1} region. The corresponding loading plots of the two regions (3400-2800 cm^{-1} and the 1740-900 cm^{-1}) are shown (Figs. 3 b and d). The loading plot that produced the separation (Fig. 3d) has shown some interference from the uncompensated water vapor in the PCA highlighted by the spikes in the 1740-1400 cm^{-1} region. Cutting out this region to 1400-900 cm^{-1} did not show significant changes to the sample's separation or the resultant PC loading (Figs. 3 e and f) demonstrating that the water vapor interference did not have a significant impact on the PCA. The PCA loadings from the 1740-900 cm^{-1} and the 1400-900 cm^{-1} regions showed peaks at 1240 cm^{-1} and 1094 cm^{-1}, indicating that the difference between the uninfected cells in infected culture *versus* cells in uninfected control culture are at the DNA region. The control group had the same + or - sign for the score and loading in the PCA of the second derivative.

3.2. Cell viability and cycling

To investigate whether the changes in the chemical composition of host cells was a response to the parasite infection, and not due to stress-induced cytotoxic response of host cells, viability and cell cycle of the infected cells were determined at the same time that infected and control cultures were subjected to FTIR measurement. The viability of *T. gondii*-infected hBMECs was determined at 3, 6, 24, and 48 hpi by the colorimetric MTT assay. The results showed that viable host cells remaining following *T. gondii* infection was not reduced significantly compared to control cells up to 24 hpi, probably to support early survival of infected host cells. However, at 24 and 48 hpi viability of infected cells was reduced significantly compared to control uninfected cells (Fig. 4).

We harvested infected and control cells at different time points post-infection, and the nuclear DNA was stained with propidium iodide (PI) before analysis by flow cytometry. The Wilcoxon rank-sum test was used to assess differences in cell percentage in each phase of the cell cycle. Our results showed that the numbers of infected cells in S and G2/M phases were significantly higher compared to uninfected cells at 24 hpi (p value < 0.05), suggesting that *T. gondii* infection resulted in cell cycle arrest at S and G2/M phases (Fig. 5). These results indicate that manipulation of cell cycle progression is an important strategy exploited by *T. gondii* to create conducive cellular conditions for parasite replication.

3.3. Levels of extracellular amino acids

To determine whether the infection-induced alteration in cell protein balance, detected by FTIR imaging, was mediated by amino acid dyshomeostasis, the amino acid profiles of culture medium of infected *versus* uninfected cell cultures were analyzed at 0, 3, 6, 24, 48, 72, and 96 hpi using GC-MS. Our analysis identified amino acid patterns associated with *T. gondii* infection and detected significant differences (p < 0.0003) in amino acids between control and infected cultures at different time points after infection (Fig. 6). Medium of infected cultures had higher concentrations for alanine (ALA) and sarcosine (SAR) at 72 and 96 hpi; and lysine (LYS) at 96 hpi. However, medium from infected cultures had lower concentrations for alpha Amino-Butyric Acid (ABA) at 48 hpi and for asparagine (ASN) at 48, 74 and 96 hpi. For each amino acid we considered the most significant time point. The volcano plot shows the effect size, the difference in amino acid

levels between control and infected cells, against the corresponding *p*-value for testing significant differences (Fig. 7). The horizontal line shows the threshold of significance. Although Glutamine (GLN) had the largest difference, the variability was also large and thus the difference was not significant. ASN had the most significant result, with infected cells having a lower concentration at 72 hpi.

We also performed unsupervised hierarchical clustering analysis of the amino acid concentrations. The dendrograms illustrated separation of the samples based on the average concentration of amino acids in control and infected samples at 0, 3, 6, 24, 48, 72, and 96 hpi. The heatmap provided a graphical display of the temporal changes in the concentration of each amino acid, with one line for the average control culture (Con) and one line for the average infected culture (Inf). For most amino acids, the control and the infected cells are paired together. For ASN, the control and infected were far apart, indicating a clear differential response. The lines are ordered according to cluster analysis - with GLN, which had the largest absolute values at the top going down to alpha-Aminoadipic acid (AAA), which had the smallest absolute values (Fig. 8). Next, the dendrogram (tree) in the heatmap was cut to produce seven different groups. The mean (+/- 1 s.d.) of the individual replicates of the amino acids that constituted each group were plotted at 0, 3, 6, 24, 48, 72 and 96 hpi. Likewise, only ASN was split between different groups. The members of each group plot are shown (Fig. S3).

3.4. Cell metabolomics signatures along the course of infection

GC-MS-based metabolomics was used to examine the metabolic alterations in host cells in response to *T. gondii* infection. The PCA scores of this untargeted metabolomic analysis revealed distinct metabolome profiles of the different samples at 3, 6, 24 and 48 hpi, and QC sample (Fig. S4). However, non-significant differences in the levels of metabolites between infected and uninfected samples imply that either these results are a product of growth of the host cells or a limitation of sample preparation or processing. Representative examples of the measured metabolites, including myristic acid, stearic acid, carnitine, leucine, isoleucine, and cholesterol trimethylsilyl ether are shown (Fig. S5).

3.5. *T. gondii* upregulated interferon signaling and reduced cell cycle-related gene expression

Total RNA from control and infected host cells at 6, 24 and 48 hpi were analyzed using microarray technology. At 6 hpi, 383 probe sets were differentially expressed, including 306 down-regulated and 77 up-regulated. Out of the 306 down-regulated probe sets, only 285 mapped to known genes and out of 77 up-regulated probe sets only 71 mapped to known genes. The three most down-regulated genes were TXNIP (thioredoxin interacting protein; log2 FC = -3.134), KIAA1107 (uncharacterized Protein KIAA1107; log2 FC = -2.879), and DBP (D-box binding PAR bZIP transcription factor; log2 FC = -2.631); whereas the three top up-regulated genes were EFNB2 (ephrin B2; log2 FC = 1.880), CXCL8 (C-X-C motif chemokine ligand 8; log2 FC = 1.683), and ACTBL2 (actin, beta like 2; log2 FC = 1.629).

At 24 hpi, 47 probe sets were differentially expressed, including 26 down-regulated and 21 up-regulated. Out of 26 down-regulated probe sets, 24 matched to known genes, whereas all 21 upregulated probe sets matched to known genes. The three most down-regulated genes were TXNIP (thioredoxin interacting protein; log2 FC = -1.576), GBP2 (guanylate binding protein 2; log2 FC = -1.491) and ERP27 (endoplasmic reticulum protein 27; log2 FC = -1.342), whereas the three top up-regulated genes were IFIT1 (interferon induced protein with tetratricopeptide repeats 1; log2 FC = 2.515), IFI44L (interferon induced protein 44 like; log2 FC = 2.256), and IFI6 (interferon alpha inducible protein 6; log2 FC = 2.146).

At 48 hpi, 4,055 probe sets were differentially expressed with 3,653 down-regulated and 402 up-regulated. Out of 3,653, 3,400 probe sets match to known genes and out of 402 down-regulated probe sets, 314 matched to known genes. The three most down-regulated genes included ZNF451 (zinc finger protein 451; log2 FC = -4.417), CDC6 (cell division cycle 6; log2 FC = -3.941) and SLC7A6 (solute carrier family 7 member 6; log2 FC = -3.859); whereas the three top up-regulated genes included OR2T5 (olfactory receptor family 2 subfamily T member 5; log2 FC = 3.654),

LOC441268 (uncharacterized LOC441268; log2 FC = 3.402) and DBP (Dbox binding PAR bZIP transcription factor; log2 FC = 3.330). Pathways mostly associated with the differentially expressed genes included cell cycle, mitotic (Log2 FC,-1.024) and interferon Signaling (Log2 FC, 1.154).

4. Discussion

In vivo metabolomics investigations have revealed considerable information about the chemical alterations that occur in mice during *T. gondii* infection. [21, 22] Despite remarkable progress in understanding the metabolomic changes associated with toxoplasmosis in mouse models, many aspects of the chemical milieu inside host cells infected by this parasite remains unknown. This is partly due to some technical challenges that restrict our ability to reveal the full spectrum of the host cell chemical composition during infection at a suitable resolution. Raman micro-spectroscopy (RMS) has been used to probe chemical changes in host cells infected with *T. gondii*. [23] RMS combined with isotope-labelling of the amino acid phenylalanine (L-Phe(D8)) has been used to monitor nutrient acquisition by *T. gondii* infecting host cells treated with Deuterated Phe (L-Phe(D8)).[24] This targeted metabolite measurement although enabled seamless monitoring of single molecule trafficking between the host cell and the parasite at a single cell scale, it does not allow global analysis of chemical changes that occur in host cells.

The FTIR spectroscopy has been an established technique for a number of research fields including cancer research, at a single cell level. [25] However, the medical infectology community is less aware of its immense potential. Also, the application of infrared spectroscopy methods to host-parasite interaction research is a relatively new development.[7] Here, we performed a quantitative analysis of *T. gondii*-related, time-dependent changes of the major chemical classes in infected hBMECs. We used microFTIR system to profile the chemical composition of hBMECs before and at different time points after infection with *T. gondii*. Our analysis revealed that naïve (uninfected) and infected cells exhibit distinct molecular profiles and that the levels of protein, lipid and nucleic acid, but carbohydrate, have been affected in response to infection. These findings are consistent with results described previously in mice, underscoring the important roles of lipid, protein and nucleic acid in *T. gondii* infection. [21, 22]

PCA of the IR spectra revealed a reduction in the protein level (3289 cm^{-1}, 2963 cm^{-1}, 2875 cm^{-1}) in infected cells (Fig. 1) and GC-MS amino acid profiling uncovered a reduction in the levels of some amino acids in the medium of infected cells (Fig. 6). GC-MS profiling of the culture medium showed a reduction in alpha Amino-Butyric Acid (ABA) at 48 hpi and in asparagine (ASN) at 48, 74 and 96 hpi. Although *T. gondii* parasites can produce asparagine *de novo*, they seem to acquire more asparagine form the surrogate host cells. This result is anticipated because amino acids are crucial nutrients for *T. gondii* and required for protein synthesis and generation of metabolic intermediates essential for its survival and replication.[26] *T. gondii* parasites possess five cathepsin-like proteases including one cathepsin L (TgCPL), one cathepsin B (TgCPB), and three cathepsin Cs (TgCPC1, -2, and -3). TgCPB co-localizes with TgCPL in the parasite endolysosome-like vacuolar compartment, and play role in the degradation of host cell proteins. [27] Protein acquisition from the host cytosol and degradation by *T. gondii* does not seem to be limited to a particular type of host protein or to parasite strain virulence.[28] Therefore, reduction in protein level in infected cells might be caused by the increased consumption of amino acids in parasite anabolism,[29,30] allowing *T. gondii* to acquire amino acids without the need to utilise its endogenous biosynthesis machinery.

A large effect on host cell arginine concentration was expected given that the parasites are auxotrophic for arginine.[28] However, arginine was not detected in this study because detection of arginine requires the use of Liquid Chromatography (HPLC) kit option, but in the present study we used the Gas Chromatography kit, which does not quantify arginine. Findings obtained in the present and previous studies[28] support the assumption that growth and proliferation of *T. gondii* can adversely impact the biosynthetic capabilities of the host due to competition for essential and growth limiting amino acids. Our result raises an interesting question as to whether the measured reduction in protein signal by microFTIR is due to parasite

consumption or reduced cellular protein synthesis. In the future, we intend to investigate this hypothesis using techniques that allow actual measurement of protein synthesis, such as stable isotope labelling combined with peptide mass spectrometry analysis, or ribosome analysis.

T. gondii manipulates cell cycle regulators in order to induce host cell cycle arrest at G2/M phase [31,32] and thus maintain its survival in the host cell cytoplasm within the PV. Our results showed that cell cycling was inhibited in infected cells at S and G2/M phases at 24 hpi (Fig. 5). This finding is supported by the gene expression analysis where cell cycle, mitotic pathway was found to be the most downregulated pathway in infected cells at 24 hpi (Log2 FC, -1.024). Results of our data therefore support earlier observations reported in other cell types.[31-33] *T. gondii* dense granule protein *GRA16*, which traffics to the host cell nucleus, [34] can potentially via downregulation of cyclin-B, lead to G2 arrest. In *T. gondii*-infected human fibroblast and trophoblast cells, Ubiquitin-like with PHD and ring finger domains 1 (UHRF1) is required for progression of the cell cycle towards the G2/M phase, which provides a suitable microenvironment for growth of the parasite. [32] The cell cycle of infected fibroblasts and trophoblasts was arrested in G2/M [32,33] which was correlated with decreased expression of UHRF-1 and cyclin B1.

This parasite has been also thought to induce cell arrest through epigenetic and transcriptomic dysregulation.[35] UHRF1 affects epigenetic modifications, including DNA methylation, histone methylation, and chromatin remodelling. *T. gondii* may exploit UHRF1 to control the host cell epigenetic machinery.[36] Cell cycle arrest or prolonging G2-phase of *T. gondii*-infected cells is apparently beneficial to the parasite to complete its growth cycle within the host cell. The G2/M-phase arrest is likely to provide the parasites with an active environment to facilitate its proliferation independent of host cell replication. It might be argued that the reduced level of protein in infected cells is due to less number of cells in infected culture compared to that in the control (uninfected) culture. However, this assumption is unlikely because our analysis was based on single cells and involved equal number of infected and uninfected cells.

We detected increased IR absorbance for lipids (2853 cm^{-1}) in infected cells compared to uninfected cells. Lipids are essential for the parasite invasion and proliferation within host cells.[4,37] Metabolic profiling also revealed a slight increase in the level of two fatty acids, myristic and stearic. These fatty acids seem to inhibit the production of tumor necrosis factor alpha (TNF-α),[38] which has immunoinflammatory activity against *T. gondii*. This finding is supported by the microarray results, which showed that the immune-related interferon signaling genes were the most unregulated in infected cells compared to uninfected cells at 24 hpi. The level of the osmolyte carnitine was also found slightly higher in infected cells at 48 hpi. The propionyl-L-carnitine was detected in a higher level in the brain of *T. gondii*-infected mice compared to uninfected mice.[21] Carnitine has been involved in ATP production in the protozoan *Trypanosoma brucei brucei*.[39] The three metabolites (myristic acid, stearic acid and carnitine) lack any chemical similarity that would suggest a common mechanism for their increase. However, it has been suggested that fatty acid oxidation pathway seems to be a possible biochemical link connecting carnitine and fatty acids because the conjugation of fatty acids to carnitine is required for transport of long-chain fatty acids across the mitochondrial membranes.[40] Given their important biological functions, the modestly high levels of these metabolites in infected cells at 48 hpi suggest that they may contribute to the parasite interaction with the host cell.

We also detected increased IR absorbance of the spectral bands that have been assigned to nucleic acids (976 cm^{-1}, 1097 cm^{-1} and 1245 cm^{-1}) in infected cells compared to uninfected cells. A previous study of the effect of the anti-cancer doxorubicin drug, which is known to cause DNA disintegration, on cancer cells has shown significant alterations in the relative absorbance of three peaks, [41] which are very similar to the nucleic acid peaks observed in the present study. The source of the nucleic acids, parasite or host origin, is unknown. However, the increase in the abundance of nucleic acids was found to increase in tandem with the growth of parasite, suggesting that the source of the nucleic acids to be of a parasite origin. Increased levels of metabolite intermediates

in the purine metabolism were detected in mouse brain infected with *T. gondii*, compared to uninfected mice. [21] Also, *T. gondii* utilizes both *de novo* and salvage pyrimidine nucleotide biosynthetic pathways for DNA/RNA biosynthesis. [42,43] The *de novo* pyrimidine biosynthetic pathway seems more important than the salvage pathway and is essential for *T. gondii* growth and virulence.[43]

A previous study has shown that during the S phase of the cell cycle, the relative intensity of protein absorption was decreased, whereas the relative concentration of nucleic acid increased slightly and the lipid concentration increased dramatically.[44] Interestingly, results of the present and previous studies, [30] showed that *T. gondii* can promote S phase of the cell cycle followed by an arrest towards the G2/M phase. These results suggest that the apparent increase in the DNA and lipid signals might be, in part, related to cell cycling. It is worth mentioning that the acquisition of spectra of hydrated cells can provide sharper, more intense bands in the DNA and lipid regions of the spectrum. [44] However, the observed changes in the DNA spectra are very unlikely to be attributed to (de)hydration effects from fixation because although all samples have been fixed using the same method, a variation in the abundance of DNA was still discernible between infected and uninfected cells.

It was interesting to observe that some host cells within infected culture resist the parasite invasion and remain parasite-free. These parasite-free cells present in the infected culture exhibited a chemometric signature that was different from uninfected host cells in control, uninfected, culture (Fig. 3). This result indicates that the metabolism of host cells growing in infected culture even if they are not physically infected by the parasite can be altered. It is possible to assume that some communication processes exist between *T. gondii*-infected and neighboring uninfected naïve host cells, possibly via signaling molecules (e.g. exosomes) [45, 46] or through secretion of protein from specialized parasite organelles, such as ROP and MIC, [31, 32] to alert naïve cells to the presence of the parasite so that they can mount an adequate immune response to counter potential parasite attack. Also, it is possible that *T. gondii* tachyzoites do not invade every cell into which they inject rhoptry material – the so called "kiss and spit" model.[47] The capacity to understand the differences in the chemical signatures representing infected and uninfected host cells has advanced our knowledge of the metabolic changes that mediate the parasite interaction with host cells.

Concluding thoughts

We have shown that microFTIR analysis can afford the needed sensitivity to analyze the chemical changes within infected cells over the intracellular replication cycle of *T. gondii*. The study findings provide new insights into how *T. gondii* remodels the chemical composition of infected host cells, by decreasing the protein and increasing the lipid and nucleic acid content of infected cells. Our data also characterized the quantitative variations in the kinetics of the extracellular levels of amino acids during infection, enhancing current understanding of amino acid dysregulation in toxoplasmosis. We acknowledge that although infrared spectroscopic approach has shown interesting results, it also has some limitations. Because it's not possible to distinguish the host or parasite origin of the detected macromolecule signals, it is not possible to make a conclusion about which of the observed changes is due to changes in the host cell or simply due to the parasite itself. It seems logical that the increase in nucleic acids and lipids is due to the replicating parasites. However, because cells vary in their biomass composition (lipids, protein, DNA content) during phases of the cell cycle, it remains unclear if the increase in DNA and lipid, and the decrease in protein signal is simply an effect of parasite replication and other cellular processes, such as the formation of the parasitophorous vacuole. Future studies should aim to measure the signature of parasites alone, and using subcellular spatial resolution FTIR approach to image the infected host cell,[48] in order to reveal what changes are inflicted upon the host cells subsequent to infection.

Funding

The authors gratefully acknowledge the support provided by Diamond Light Source for access to beamline B22 (proposal number SM9440) that contributed to the FTIR results presented in the manuscript.

Conflicts of interest

There are no conflicts to declare.

Acknowledgements

The authors thank anonymous reviewers for critical comments and suggestions.

References

1 H M. Elsheikha, *Pubic Health* 2008, **122**, 335–353.
2 J.G. Montoya and O. Liesenfeld, *The Lancet* 2004, **363**, 1965–1976.
3 J. L. Wang, H. M. Elsheikha, W. N. Zhu, K. Chen, T. T. Li and D. M. Yue*, et al., Front. Immunol.* 2017, **8**, 730.
4 C. E. Caffaro and J. C. Boothroyd, *Eukaryotic Cell* 2011, **10**, 1095–1099.
5 J. P. Boyle and J. R. Radke, *Int. J. Parasitol.* 2009, **39**, 903–914.
6 E. Kaznowska, J. Depciuch, K. Łach, M. Kołodziej, A. Koziorowska, J. Vongsvivut, *et al., Talanta* 2018, **186**, 337–345.
7 A. Khoshmanesh, M. W. Dixon, S. Kenny, L. Tilley, D. McNaughton and B. R. Wood, *Anal. Chem.* 2014, **86**, 4379–4386.
8 V. Erukhimovitch, M. Talyshinsky, Y. Souprun and M. Huleihel, *Methods Mol. Biol.* 2005, **292**, 161–172.
9 F. T. Lee-Montiel, K. A. Reynolds and M. R. Riley, *J. Biol. Eng.* 2011, **5**, 16.
10 H. M. Elsheikha, B. M. Rosenthal, A. J. Murphy, D. B. Dunams, D. A. Neelis and L. S. Mansfield, *Vet. Parasitol.* 2006, **135**, 223–234.
11 H. M. Elsheikha, C. Mckinley, N. A. Elsaied and P. A. Smith, *Parasit. Vectors* 2013, **6**, 24.
12 G. Bellisola, M. Della Peruta, M. Vezzalini, E. Moratti, L. Vaccari, G. Birarda, *et al., Analyst*, 2010, **135**, 3077–3086.
13 R. M. Jarvis, D. Broadhurst, H. E. Johnson, N. O'Boyle and R Goodacre, PyChem - a multivariate analysis package for Python. *Bioinformatics* 2006, **22**, 2565–2566.
14 M. AlKurashi, F. A. Eastick, S. V. Kuchipudi, C. Rauch, A. Madouasse, X. Q. Zhu, *et al., Vet. Parasitol.* 2011, **177**, 267–274.
15 P. Rhodes, J. Craigon, C. Gray, S. M. Rhind, P. T. Loughna and D. S. Gardner, *PLoS ONE* 2009, **4**, e7393.
16 K. D. Sinclair, L. A. Lunn, W. Y. Kwong, K. Wonnacott, R. S. Linforth and J. Craigon, *Reprod. Biomed. Online* 2008, **16**, 859–868.
17 W. B. Dunn, D. Broadhurst, P. Begley, E. Zelena, S. Francis-McIntyre, N. Anderson, *et al., Nat. Protoc.* 2011, **6**, 1060–1083.
18 D. C. Wedge, J. W. Allwood, W. Dunn, A. A Vaughan, K. Simpson, M. Brown, *et al., Anal. Chem.* 2011, **83**, 6689–6697.
19 F-N. Fu, D. B. Deoliveira, W. R. Trumble, H. K. Sarkar and B. R. Singh, *Appl. Spectrosc.* 1994, **48**, 1432–1441.
20 S. Cai and B. R. Singh, *Biophys. Chem.* 1999, **80**, 7–20.
21 C. X. Zhou, D. H. Zhou, H. M. Elsheikha, G. X. Liu, X. Suo and X. Q. Zhu, *PLoS ONE* 2015, **10**, e0139635.
22 C. X. Zhou, D. H. Zhou, H. M. Elsheikha, Y. Zhao, X. Suo and X. Q. Zhu, *Sci. Rep.* 2016, **6**, 19557.
23 A. Naemat, H. M. Elsheikha, A. Al-Sandaqchi, K. Kong, A. Ghita and I. Notingher, *Analyst* 2015, **140**, 756–764.
24 A. Naemat, H. M. Elsheikha, R. A. Boitor and I. Notingher, *Sci. Rep.* 2016, **6**, 20811.
25 S. Gok, O. Z. Aydin, Y. S. Sural, F. Zorlu, U. Bayol and F. Severcan, *J. Biophotonics.* 2016, **9**, 967–975.
26 E. Rajendran, S. V. Hapuarachchi, C. M. Miller, S. J. Fairweather, Y. Cai, N. C. Smith, *et al., Nat Commun.* 2017, **8**, 14455.
27 S. Tymoshenko, R. D. Oppenheim, R. Agren, J. Nielsen, D. Soldati-Favre and V. Hatzimanikatis, *PLoS Comput. Biol.* 2015, **11**, e1004261.
28 Z. Dou, I. Coppens and V. B. Carruthers, *J. Biol. Chem.* 2013, **288**, 3523-34.
29 Z. Dou, O. L. McGovern, M. Di Cristina and V. B. Carruthers, *MBio.* 2014, **5**, e01188–14.
30 R. E. Molestina, N. El-Guendy and A. P. Sinai, *Cell Microbiol.* 2008, **10**, 1153–1165.
31 J. Brunet, A. W. Pfaff, A. Abidi, M. Unoki, Y. Nakamura, M. Guinard, *et al., Cell Microbiol.* 2008, **10**, 908–920.
32 Y. Cai, H. Chen, X. Mo, Y. Tang, X. Xu, A. Zhang, *et al., Cell Signal.* 2014, **26**, 1204–1212.
33 A. Bougdour, E. Durandau, M.P. Brenier-Pinchart, P. Ortet, M. Barakat, S. Kieffer, *et al.*, *Cell Host Microbe* 2013, **13**, 489–500.

34 N. A. Wijetunga, A. D. Johnston, R. Maekawa, F. Delahaye, N. Ulahannan, K. Kim *et al.*, *BMC Bioinformatics* 2017, **18**, 41.

35 M. Unoki, J. Brunet and M. Mousli, *Biochem. Pharmacol.* 2009, **78**, 1279–1288.

36 I. Coppens and K. A. Joiner, *Mol. Biol. Cell.* 2003, **14**, 3804–3820.

37 F. Debierre-Grockiego, K. Rabi, J. Schmidt, H. Geyer, R. Geyer and R. T. Schwarz, *Infect. Immun.* 2007, **75**, 2886–2893.

38 R. Gilbert and R. A. Klein, *FEBS Lett.* 1982, **141**, 271–274.

39 W. R. Wikoff, G. Pendyala, G. Siuzdak and H. S. Fox, *J. Clin. Invest.* 2008, **118**, 2661–2669.

40 L. M. Weiss and K. Kim, *Int. J. Parasitol.* 2004, **34**, 249–252.

41 P. L. V. Fale, A. Altharawi and K. L. A. Chan, *BBA-Mol. Cell Res.,* 2015, **1853**, 2640–2648.

42 I. Coppens, T. Asai and S. Tomavo, in *Toxoplasma gondii* (Second Edition), ed. L. M. Weiss and K Kim, Academic Press, Boston, 2nd ed, 2014, vol. 1, ch. 8, pp. 257–295.

43 M. J. Kim, B. K. Jung, J. Cho, H. Song, K.H. Pyo, J. M. Lee, *et al.*, *Korean J. Parasitol.* 2016, **54**, 147–154.

44 D. R. Whelan, K. R. Bambery, L. Puskar, D. McNaughton, and B. R. Wood, *Analyst* 2013, **138**, 3891–3899.

45 Y. Li, F. Xiu, Z. Mou, Z. Xue, H. Du, C. Zhou, *et al.*, *Nanomedicine (Lond)*. 2018, **13**, 1157–1168.

46 M. D. Lavine and G. Arrizabalaga, *Mol. Biochem. Parasitol.* 2009, **164**, 95–99.

47 J. C. Boothroyd and J. F. Dubremetz, *Nat. Rev. Microbiol.* 2008, **6**, 79–88.

48 K. L. A. Chan, P. L. V. Fale, A. Atharawi, K. Wehbe and G. Cinque, *Anal. Bioanal. Chem.* 2018, **410**, 6477–6487.

.

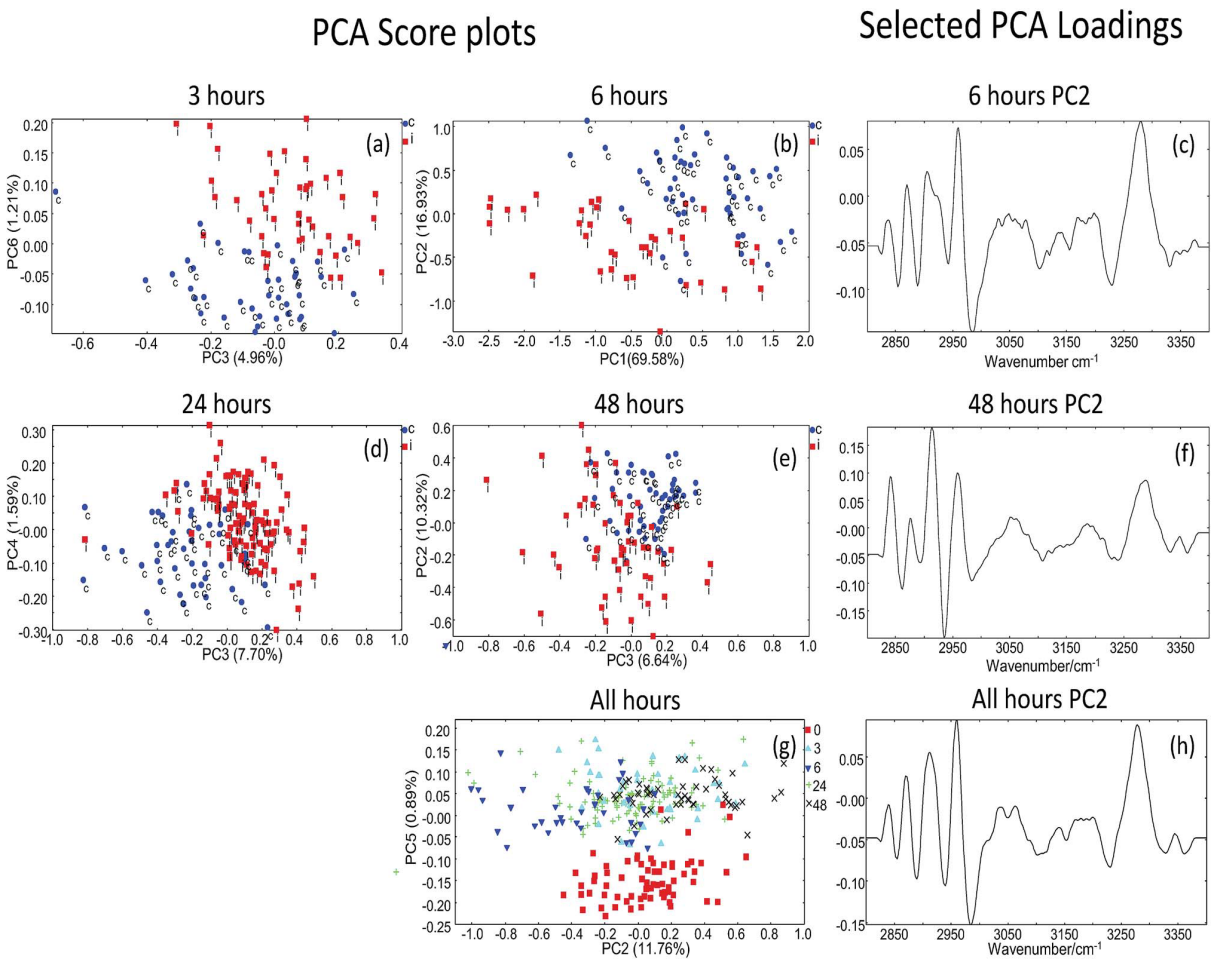

Fig. 1 (a-f) The score and loading plots of the PCA of infected (red■) and control (blue•) hBMECs at various time points after infection in the 3400–2800 cm^{-1} region. (g-h) The PCA of the spectral data from all time points where 0, 3, 6, 24 and 48 hours are respectively denoted by red ■, turquoise ▲, blue ▼, green + and black + symbols.

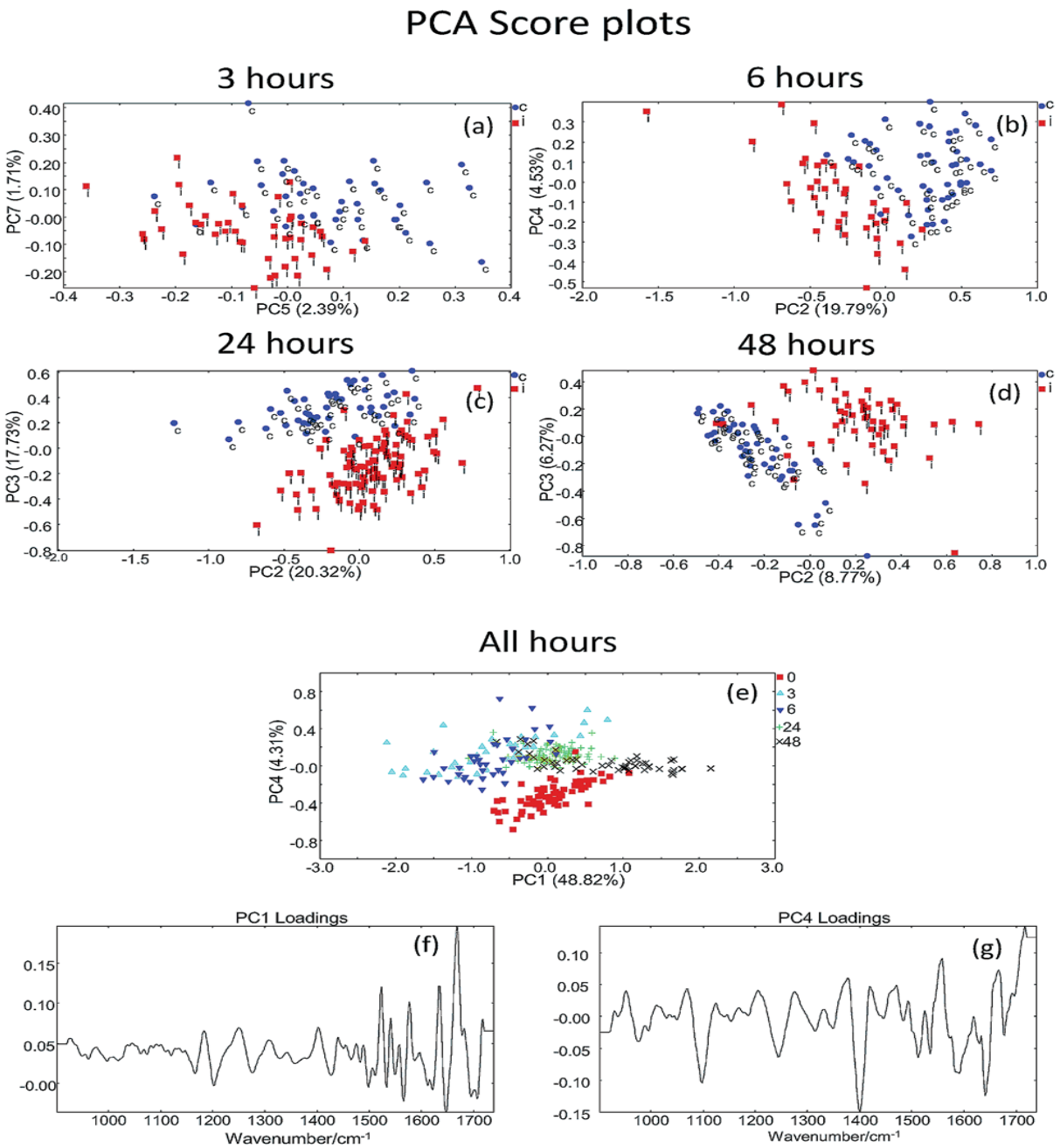

Fig. 2 (a-d) The score and loading plots of the PCA of infected (red■) and control (blue•) hBMECs at various time points postinfection in the 1740–900 cm^{-1} region. (e-g) The PCA of the spectral data from all time points where 0, 3, 6, 24 and 48 hours are respectively represented by red ■, turquoise ▲, blue ▼, green + and black + symbols.

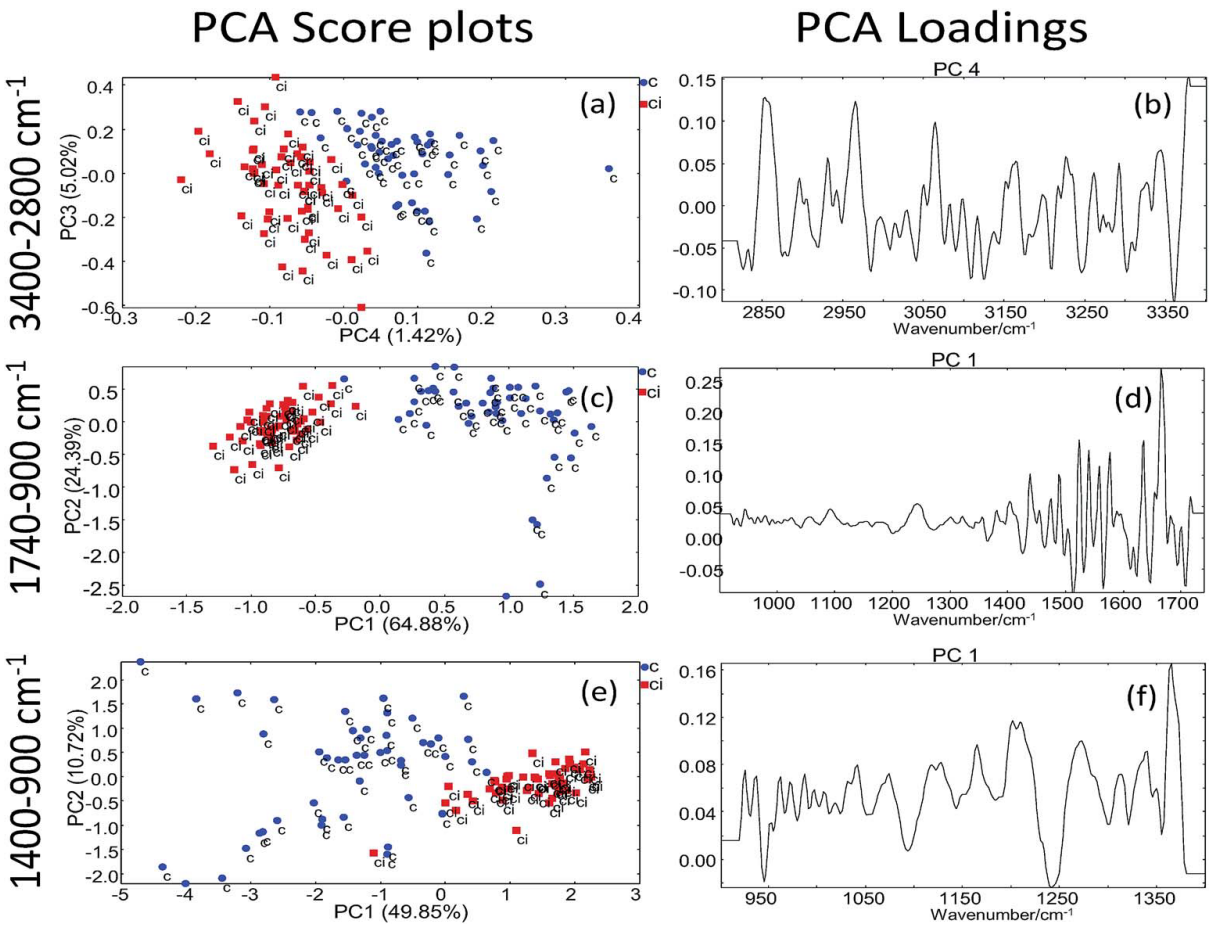

Fig. 3 The score and loading plots of the PCAs of the healthy cells in the hBMEC culture infected for 48 hr (red ■) and the corresponding healthy cells in uninfected control culture (blue•).

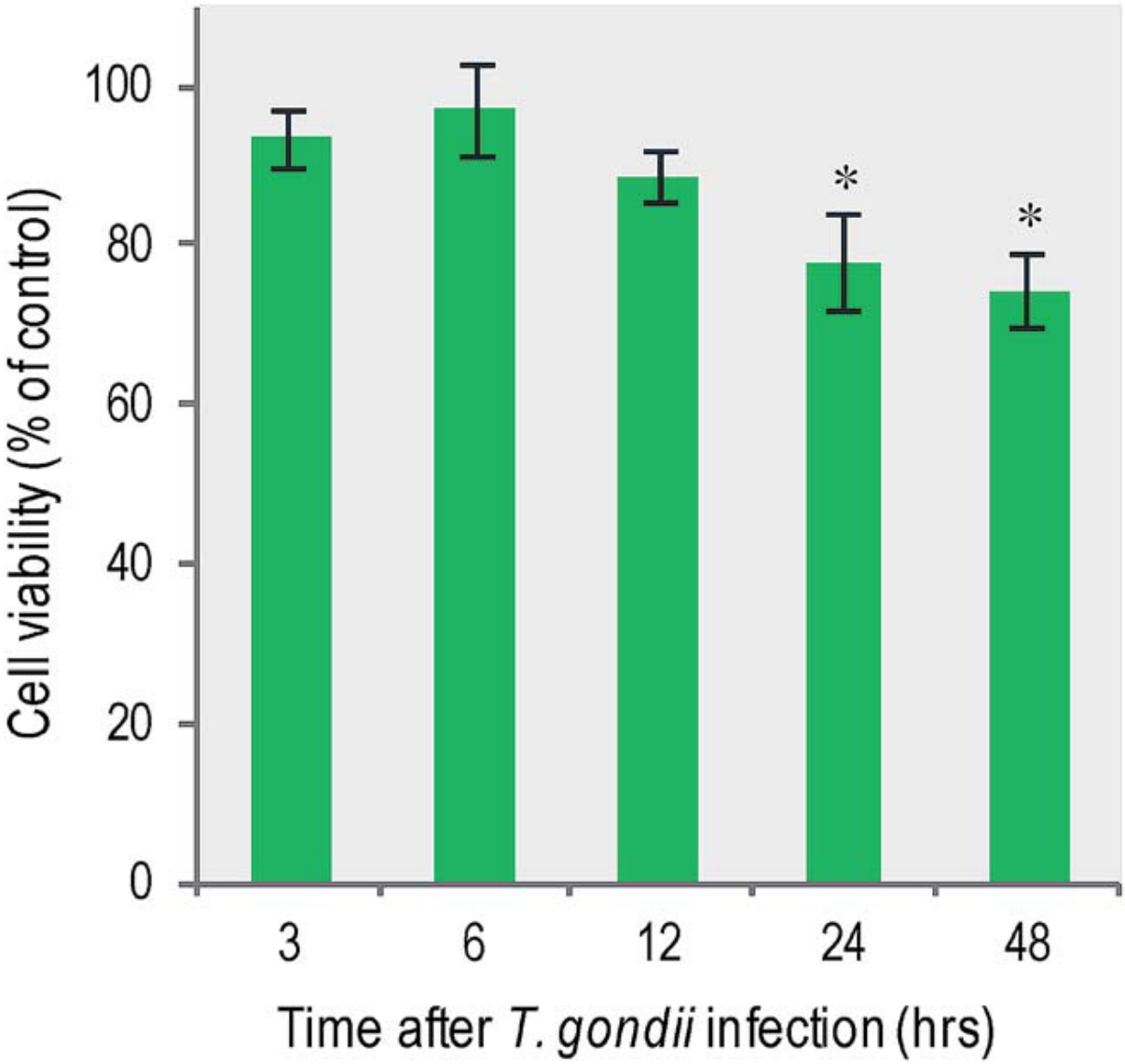

Fig. 4 The colorimetric MTT assay was used to measure the changes in the host cell viability in response to *T. gondii* infection at 3, 6, 12, 24, and 48 hours postinfection (hpi). Absorbance values decreased in proportion to time post infection, indicating gradual reduction in the viability, which was significant only at 24 and 48 hpi. Data were analyzed by one-way ANOVA with post-test Dunnette comparing the control group with each infected group (*p <0.05). Results are expressed as % of the uninfected control cells.

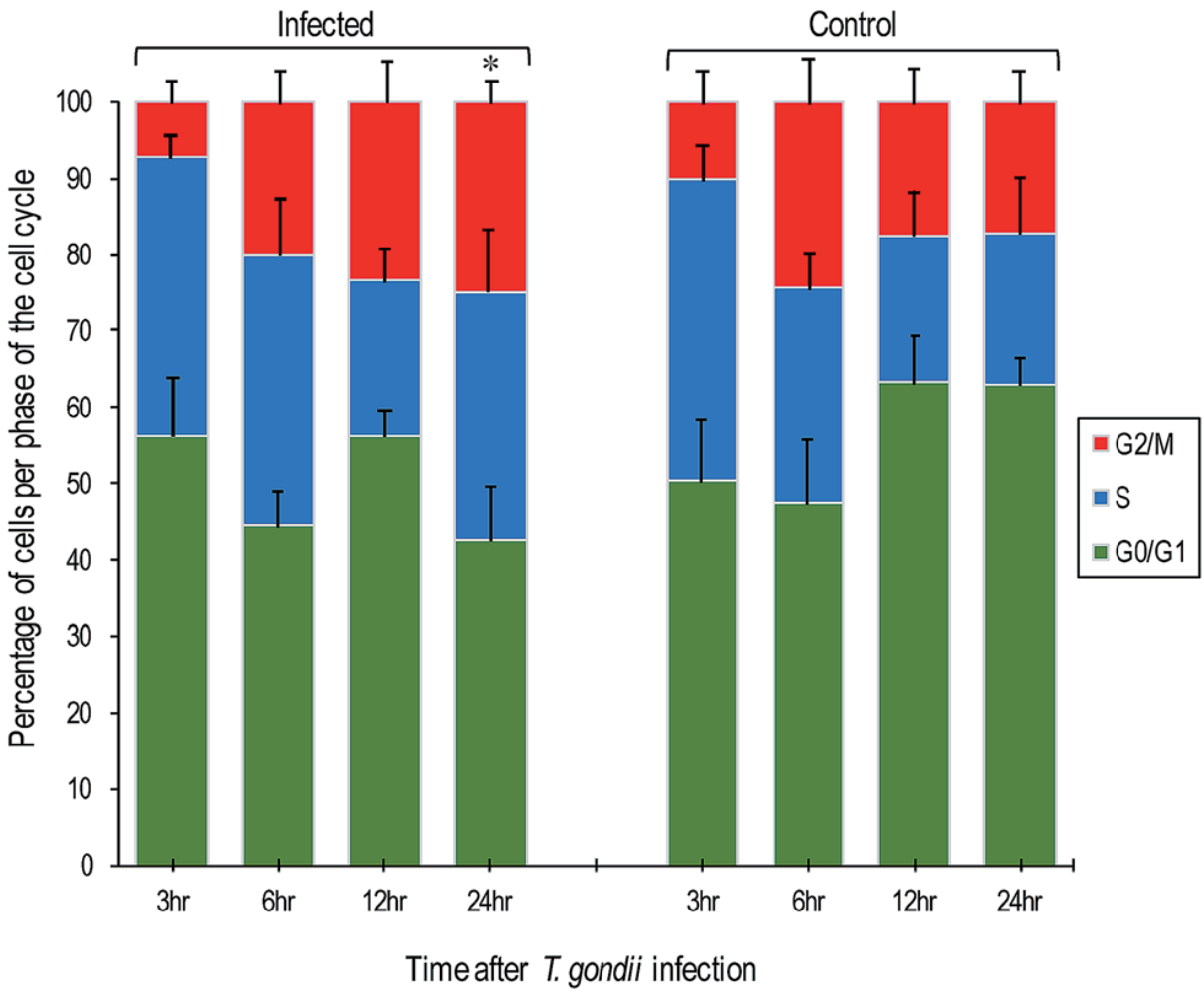

Fig. 5 The effect of *T. gondii* infection on phases of host cell cycle was determined using propidium iodide-based flow-cytometric analysis at 3, 6, 12, and 24 hr post-infection (hpi). The number of cells in each phase of the cell cycle was stratified. Cell cycle profiles showed that *T. gondii* infection significantly decreased the proportion of G_0/G_1-phase cells and significantly increased the number of cells in the S-phase and G_2/M phase only at 24 hpi. Median values are shown, with difference assessed using a Wilcoxon rank sum test (*p < 0.05).

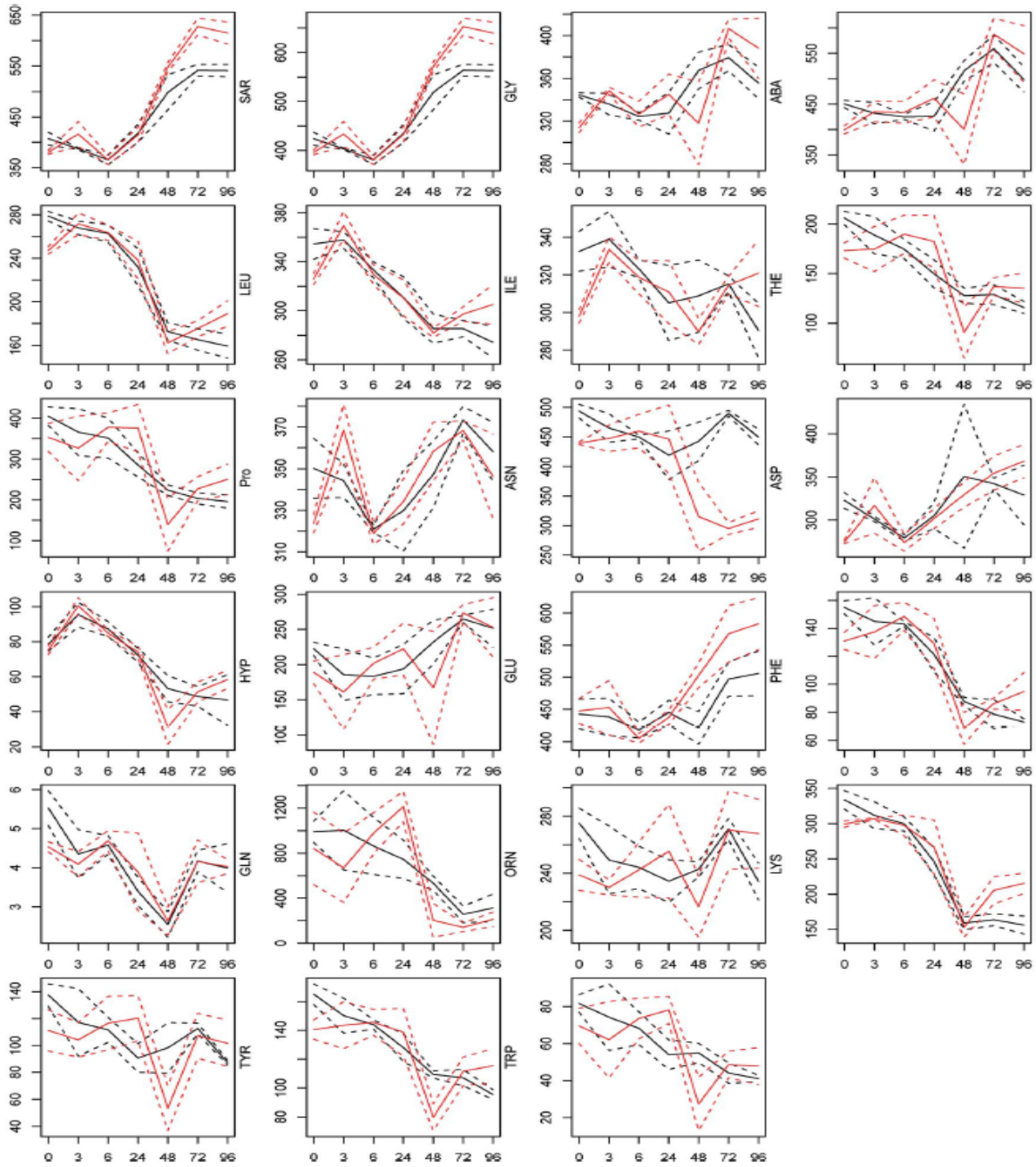

Fig. 6 Amino acids plots showing time-dependent dynamic changes in the levels of amino acids in the culture medium. Each panel shows kinetic signature of one of the 23 amino acids detected in the supernatant of hBMECs at the indicated points before and after infection with *T. gondii* RH strain. All amino acids showed a dynamic temporal behaviour at the time points after infection: 0 hour (baseline value before infection), 3, 6, 24, 48, 72, and 96 hours after infection. X-axis represents time after infection in hours and Y-axis indicates the concentration of amino acids (μM/L). Black and red solid lines represent average control and infected responses, respectively, with the dotted lines showing +/- 1 s.d. Notably, the majority of amino acids showed a similar trend for both control and infected cells. ALA, SAR and ASN displayed a clear difference, with the results for ALA and SAR being very similar.

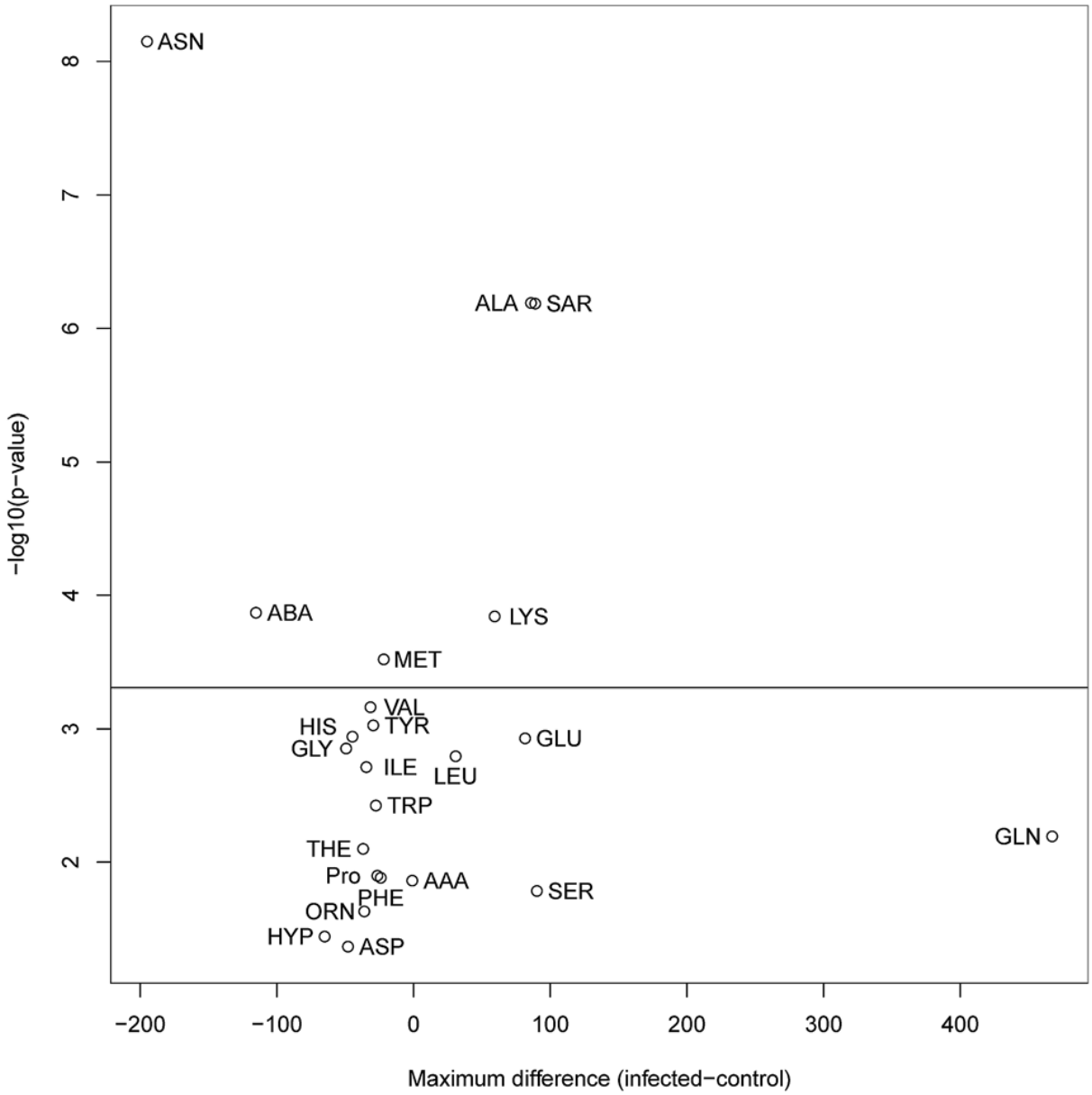

Fig. 7 Volcano plot showing the differentially abundant amino acids.. Amino acids are represented as individual circles and plotted along the x-axis by the effect size, the difference between control and infected concentration levels, and on the y-axis by the significance level, $-\log_{10}$ (*p* value). The horizontal line indicates the significance threshold after correcting for multiple tests, with amino acids above the line being significant. Only the most significant time point for each amino acid is included. ASN was the most significant result with lower concentration levels in infected cells at 72 hpi. The results for ALA and SAR are similar.

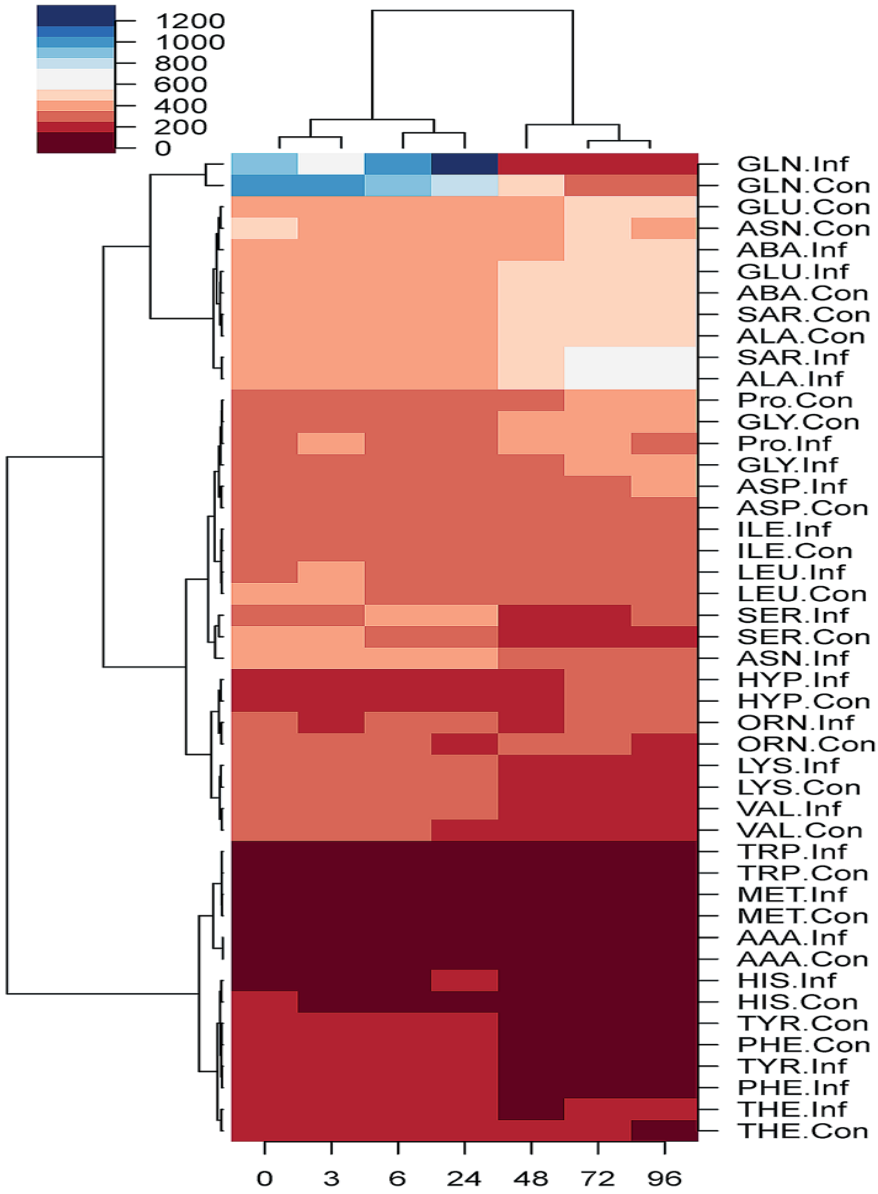

Fig. 8 A heatmap and cluster tree illustrating fluctuations in the concentration of amino acids between infected and uninfected hBMECs over the course of infection using a color-scale, with the amino acids ordered according to the cluster analysis. Average control and infected samples over the course of infection were calculated for each amino acid by taking the mean over control replicates and infected replicates. Two hierarchical cluster analyses combined with a heatmap revealed trends across time points after infection and between variables (amino acids). Each amino acid is represented by two rows, average control (Con) and average infected (Inf), and each time point is represented by a single column. Blue indicates increased amino acid level, whereas red indicates decreased level of amino acids. The dendrograms were calculated using Ward's method on Euclidean distances between the average response vectors.

Supplemental figures:

All supplementary information figures are accessible at:
http://www.rsc.org/suppdata/c8/ay/c8ay02777c/c8ay02777c1.pdf